



OPEN The therapeutic potential of pegylated arginase I treatment in glioblastoma

Marcus Kwong Lam Fung¹, Shing Chan¹, Stella Sun², Ping De Zhang², Gilberto Ka Kit Leung² & Godfrey Chi Fung Chan^{1,3}✉

This study used *in vitro* experiments and an orthotopic glioblastoma (GBM) mouse model to test the efficacy of human pegylated arginase I formulation, BCT-100, against the incurable cancer, GBM. Arginine auxotrophy in GBM was verified *in silico* and *in vitro* by absence of OTC and ASS1 expression. BCT-100 inhibited growth and induced cell death in four GBM cell lines *in vitro*. Transcriptomics of U87 and U373 treated with BCT-100 responded differently. BCT-100-treated U87 showed autophagy induction. Cytotoxicity enhancement was observed in four cell lines treated with BCT-100 + chloroquine (CQ). CQ + BCT-100 induced caspase-dependent and caspase-independent cell death in luciferase-transfected U87 (U87(lf+)). BCT-100 or CQ monotherapy, but not BCT-100 + CQ, prolonged survival of intracranial U87(lf+)-bearing mice similarly without suppressing tumor growth. Mouse microglia cell BV2 protected U87(lf+) from BCT100-induced cytotoxicity in transwell co-culture. Etoposide suppressed BV2's protection to U87(lf+) upon BCT-100 treatment by suppressing the growth and inducing cell death of BV2, suggesting microglial suppression as a strategy for enhancing the efficacy of BCT-100. Microglial protection may explain the *in vitro* and *in vivo* discrepancies. Further investigation into microglia/GBM interactions may help improve the efficacy of arginine deprivation therapy against GBM.

Keywords Arginine deprivation, Glioblastoma, Microglia, Tumor microenvironment, Pegylated arginase I, Combination therapy

Abbreviations

ASS-1	Arginino-succinate synthetase-1
CQ	Chloroquine
GBM	Glioblastoma multiforme
OTC	Ornithine transcarbamylase
TMZ	Temozolomide
XTT assay	2,3-Bis-(2-Methoxy-4-Nitro-5-Sulphophenyl)-2H-Tetrazolium-5-Carboxanilide assay

Glioblastoma (GBM) is a cancer found in the brain or spinal cord¹. It is currently incurable and may occur in people of all ages². Current treatment involves surgery, radiotherapy, and chemotherapy². Chemotherapy usually involves the use of temozolomide (TMZ) and cisplatin². Other approaches include the use of anti-angiogenesis or anti-EGFR (epidermal growth factor receptor) agents³. However, all these approaches may only prolong survival for a few months. The median overall survival of GBM remains in the range of 14 to 20 months³. Therefore, there is a need to develop novel therapeutic methods to improve the outcome of GBM¹.

Arginine is a semi-essential amino acid important for cancer cell metabolism in protein translation, cellular proliferation and synthesis of metabolites important for cancer survival, proliferation and metastasis (e.g. polyamine and nitric oxide)^{4,5}. Many cancer cells are thought to be auxotrophic for arginine based on the low or no expression of the two enzymes involved in arginine metabolism: ornithine transcarbamylase (OTC) and argininosuccinate synthetase-1 (ASS1) and require exogenous arginine for survival and growth^{6,7}. Arginine auxotrophy in GBM cells forms the basis of arginine depletion-based therapy⁸. Currently, arginine depletion

¹Department of Paediatrics & Adolescent Medicine, School of Clinical Medicine, LKS Faculty of Medicine, The University of Hong Kong, Pok Fu Lam, HKSAR, China. ²Department of Surgery, School of Clinical Medicine, LKS Faculty of Medicine, The University of Hong Kong, Pok Fu Lam, HKSAR, China. ³Paediatric Hematology & Oncology Centre, Hong Kong Sanatorium & Hospital Eastern Medical Centre, Shau Kei Wan, HKSAR, China. ✉email: gcfchan@hku.hk

occurs in two ways via two different enzymes, namely arginine deiminase (ADI) from bacteria and arginase I (Arg I) from bacteria or humans^{6,9,10}. ADI breaks down arginine into citrulline, and arginase breaks down arginine into ornithine⁶. The relevant pathways of arginine breakdown/synthesis are illustrated in Fig. 1a. In order to prolong the half-life of the enzymes in blood circulation and to reduce immunogenicity, there are pegylated forms of ADI and ARG, namely peg-ADI and peg-Arg I¹¹. In principle, peg-ADI is used to target ASS1-negative tumors, and peg-Arg I is used to target OTC-negative tumors^{12,13}. Both peg-ADI and peg-Arg I have gone through phase I clinical trials for safety studies. They demonstrated a good safety profile, and several clinical trials are ongoing to optimize their treatment efficacy^{14–16}. The good safety profile of arginine-depleting agents makes them a good candidate for new armamentarium for cancer therapy. Therefore, there have been several pre-clinical studies exploring the usage of arginine-depleting enzymes in different types of cancers¹⁷.

Arginine-depleting enzymes were reported to be effective in suppressing growth and inducing cell death in both hematologic malignancies, such as acute leukemia, and solid tumors, such as prostate carcinoma, melanoma, breast carcinoma, etc.¹³. All studies of arginine-depleting enzymes in different cancer types show tumor suppression and/or prolonged survival in tumor-bearing mice in vivo under both subcutaneous and orthotopic tumor mouse models¹⁸. In GBM, there have been in vitro, subcutaneous, and orthotopic tumor mouse model studies on the therapeutic potential of peg-ADI^{19–21}. Peg-ADI could suppress the growth of ASS1-negative GBM cell line LN229 but not ASS1-positive GBM cell line U87 in vitro. Peg-ADI also suppresses ASS1-negative tumor growth and extend survival in an immune-deficient orthotopic GBM model²¹. Peg-ADI could synergize with TMZ to suppress ASS1-negative and ASS1-positive tumor growth in an immune-deficient orthotopic GBM model²¹. It was also recently reported that peg-ADI combined with radiotherapy could significantly reduce tumor growth and prolong the survival of ASS1-positive immune-competent orthotopic GBM models²⁰. There have also been in vitro studies of chemically modified human peg-Arg I on GBM²². The chemically modified human peg-Arg I could suppress growth and induce autophagy and cell death in glioma cell lines in vitro²².

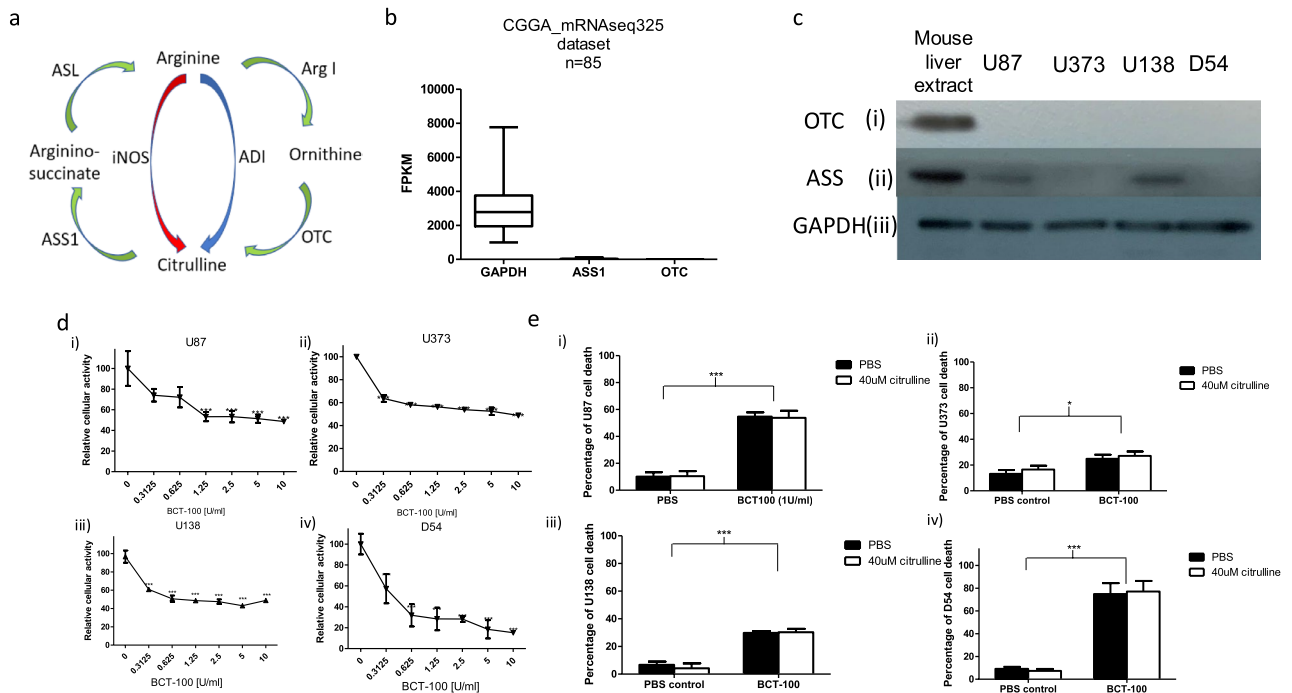


Fig. 1. Glioblastoma lacks arginine-replenishing enzymes and is chemo-sensitive to BCT-100. **(a)** Arginine metabolism. The green arrows indicate the urea cycle pathway. The red arrow indicates the arginine–nitric oxide pathway. The blue arrow indicates arginine breakdown by arginine deiminase. **(b)** RNAseq data from dataset mRNA325 of Chinese Glioma Genome Atlas of 85 first-diagnosed glioblastoma patients showing gene expression of GAPDH, OTC, and ASS1 as FPKM (fragments per kilobase of transcript per million mapped reads). **(c)** Western blotting analysis of OTC and ASS1 expression in four glioblastoma cell lines: U87, U373, U138, and D54. Mouse liver extract was used as the positive control. GAPDH was used as the loading control. The blots originated from the same protein extract separated by different gels and transferred to different blots. Such an arrangement was used because of the similar sizes of OTC, ASS1, and GAPDH, and stripping could not make the protein bands clearly distinguishable. The whole blots of Fig. (c(i)), (c(ii)), and (c(iii)) are shown in Supplementary Fig. S1a, S1b, and S1c, respectively. **(d)** (i–iv) Dose–response curve (in terms of cellular activities) of U87, U373, U138, and D54 (representative results presented with technical triplicates) treated with different concentrations of BCT-100, respectively, by using XTT assay. *** $p < 0.001$ compared to PBS. **(d)** Cytotoxicity responses of U87, U373, U138, and D54 treated with or without 1 U/ml BCT-100 and/or 40 μM citrulline by using annexin V/propidium iodide assay. * $p < 0.05$ compared to PBS. *** $p < 0.001$ compared to the PBS.

However, no study has reported the in vivo efficacy of human peg-Arg I in GBM yet. Therefore, we investigated the in vitro mechanisms and in vivo efficacy of peg-Arg I on GBM.

Methods

Cell cultures

GBM cell lines U87 (HTB-14), U373 (HTB-19), and U138 (HTB-16) were purchased from American Type Culture Collection (Virginia, USA). D54 was a gift from Duke University Medical Center, Durham, NC, USA²³. The mouse microglia cell line BV2 was provided by Prof. E Choi from the Laboratory of Cell Death and Human Diseases, Korea University. BV2, U373, U138, and D54 were cultured in Dulbecco's modified Eagle's medium (Thermo Fisher, Waltham, USA, 12100046), while U87 and luciferase-transfected U87 (U87(lf+)) were cultured in minimum essential medium (MEM)- α (Thermo Fisher, Waltham, USA, 12000063) at 37 °C in 5% CO₂ at 90% relative humidity. All media were supplemented with 10% heat-inactivated fetal bovine serum (FBS) (Hyclone, Logan, USA, SH30088.03), 100 IU/ml of penicillin, and 100 μ g/ml of streptomycin (Thermo Fisher, Waltham, USA, 15140122)²³.

Chemicals and antibodies

BCT-100 was kindly provided by Dr. Paul Cheng of Bio-Cancer Treatment Ltd. (Hong Kong SAR, China), and temozolomide (85622–93), chloroquine diphosphate (C6628), pan-caspase inhibitor z-vad-fmk (V116), and citrulline (C7629) were purchased from Sigma Aldrich (St. Louis, USA). Etoposide (33419–42-0) was purchased from Teva Limited (Toronto, Canada). α -difluoromethylornithine (DFMO) was purchased from Caymen Chemical (Ann Arbor, USA, 16889). Anti-human GAPDH (Glyceraldehyde 3-phosphate dehydrogenase) (ab9485), anti-human LC3B (ab48394), anti-human ASS1 (ab170952), and anti-human OTC (ab228646) antibodies were purchased from Abcam (Cambridge, UK). PE-conjugated anti-mouse CD86 (105007) and PE-conjugated anti-mouse CD206 (141705) were purchased from BioLegend (San Diego, USA). Anti-human p62 was purchased from Santa Cruz Biotechnology (Santa Cruz, CA, USA, sc-48402). Mouse interferon gamma (IFN- γ) (315–05) and mouse interleukin 4 (IL-4) (214–14) were purchased from PeproTech Inc. (Cranbury, USA). D-luciferin was purchased from Gold Biotechnology (St. Louis, USA, LUCK-100).

Transwell co-culture

BV2 cells were seeded at a density of 1×10^4 cells/well into a transwell insert in 12-well plates (Corning, USA, CSL3512). BV2 cells were pretreated with or without 20 ng/ml mouse IFN- γ , 100 ng/ml mouse IL-4, or 20 μ M VP-16 for 48 h in the transwell insert (Corning, USA, CSL3401). U87(lf+) cells were seeded at a density of 5×10^4 cells/well onto 12-well plates containing the drug/cytokine-pretreated BV2 cells in transwell insert. The co-cultures were incubated with MEM- α medium supplemented with 10% FBS and 1% penicillin/streptomycin at 37 °C in 5% CO₂. U87(lf+)/BV2 blasts co-culture was treated with or without 1 U/mL BCT-100 for 72 h.

XTT Assay

U87, U373, U138 and D54 were plated at 10^4 per well in 96-well plates overnight and then treated with BCT-100 of concentrations (0, 0.3125, 0.625, 1.25, 2.5, 5 and 10 U/ml) for 72 h at 37 °C in 5% CO₂. Cell viability was determined by using XTT cell proliferation assay (a colorimetric method) kit according to the manufacturer's instructions (Roche Diagnostics, Tucson, USA, 11465015001)²⁴.

Annexin V (AV)/Propidium Iodide (PI) assay

AV/PI (Annexin V-FITC Kit, Becton, Dickinson and Company, Franklin Lakes, USA, 556547) was used to assess the extent of apoptosis in glioma cell lines (U87, U87(lf+), U373, U138 and D54) after exposure to different drug treatments for 72 h (AV/PI kit partly sponsored by Bio-Cancer Treatment Ltd, Hong Kong). Glioma cell lines were harvested by trypsinization, washed, and then resuspended in 1X AV binding buffer provided by the commercial kit. The cells were labeled with annexin V-fluorescein 5(6)-isothiocyanate (AV-FITC) and PI following the manufacturer's instructions and analyzed using flow cytometry. Flow cytometric analysis was performed with a BD LSR II (BD Biosciences, San Jose, USA). A total of 10,000 events per sample were collected into list mode files and analyzed by using FlowJo.

Immunophenotyping

Mouse microglia cells BV2 were stimulated by mouse IL-4 or IFN- γ for 48 h. BV2 were then washed and incubated with cold phosphate buffered saline (PBS) for 30 min; they were then harvested by gentle scratching and centrifuged. Cell pellets were resuspended in PBS in 2% FBS and stained with PE-conjugated anti-mouse CD86-PE or anti-mouse CD206 for 15 min. Stained cells were washed to remove excess antibodies and then analyzed by using flow cytometry and BD LSR II (BD Biosciences, San Jose, USA). A total of 10,000 events per sample were collected into list mode files and analyzed by using FlowJo.

Protein extraction, SDS-PAGE, and western blotting

Protein extraction, SDS-PAGE, and Western blotting were carried out as previously described²⁴. Briefly, the cells with different treatments were lysed using radioimmunoprecipitation assay (RIPA) buffer. The protein concentration of the lysates was determined using the Bio-Rad protein assay (Thermo Fisher, Waltham, USA, 23227). A total of 25 μ g of protein from the whole cell lysate of each sample was used for 12% SDS-PAGE, and subsequently, the gels were electro-blotted onto polyvinylidene difluoride (PVDF) membranes (Immobilon-P, Millipore, Burlington, USA, IPVH00010) and blocked by 5% non-fat milk in Tris-buffered saline +0.1% overnight Tween-20 (TBS-T) (Thermo Fisher, Waltham, USA, 85113). Primary antibodies at 1: 1000 or 1:5000 (for anti-GAPDH antibody) dilution in 5% non-fat milk in TBS-T were used to stain the proteins of interest for 1.5 h

(catalogue numbers mentioned in previous part “Chemicals and antibodies”). After washing 10 times by TBS-T, horseradish peroxidase-conjugated antibodies against mouse (ab6708) and rabbit (ab6721) IgG were used as secondary antibodies at 1:5000 dilution in 5% non-fat milk in TBS-T for 1 h staining (Abcam, Cambridge, UK). After washing 10 times by TBS-T, secondary antibody binding was detected using enhanced chemiluminescence (ECL) Western detection blotting reagents (GE Healthcare, Chicago, USA, 28980926) and Fuji Medical X-Ray Film (Tokyo, Japan, 100NIF). The band intensities were analyzed using ImageJ.

Active caspases 3, 8, and 9 staining

Active caspase 3, 8, and 9 staining was carried out according to the manufacturer’s protocol. For active caspase 3 staining, after 72h drug treatments (PBS, 5 μ M CQ, 1U/ml BCT-100 or 1U/ml BCT-100 + 5 μ M CQ), U87(lf+) were harvested using trypsinization, washed, permeabilized, washed again, and then stained with active human caspase 3-FITC antibody (BD Biosciences, San Jose, USA, 550480). The stained cells were then washed again before analysis using flow cytometry. For active caspase 8 and 9 staining, briefly, after 72h drug treatments (PBS, 5 μ M CQ, 1U/ml BCT-100 or 1U/ml BCT-100 + 5 μ M CQ), U87(lf+) were harvested using trypsinization, washed, and stained by FITC-conjugated caspase inhibitor FITC-IETD-FMK for caspase 8 (Abcam, Cambridge, UK, ab65614) and FITC-LEHD-FMK for caspase 9 (Abcam, Cambridge, UK, ab65615). The stained cells were also washed before analysis using flow cytometry.

RNA extraction, transcriptome sequencing, and data analysis

The U87 and U373 cell lines were seeded at a density of 3×10^5 cells/well in six-well plates overnight and treated with PBS or BCT-100 for 72 h. The cells were lysed in TRIzol™ Reagent (Thermo Fisher Scientific, Waltham, USA, 15596026) for RNA extraction according to the manufacturer’s instructions. RNA with an RNA integrity number ≥ 8 was used for non-strand-specific RNA library preparation using the poly-A tailed capture method with the KAPA mRNA HyperPrep Kit (Roche Diagnostics, Tucson, USA, 08098123702) according to the manufacturer’s protocol. RNA libraries were sequenced as 150 bp paired-end runs on an Illumina NovaSeq 6000 platform (Illumina, San Diego, CA, USA) with a minimum of 100 million reads per sample at the Center for PanorOmic Sciences (CPOS), University of Hong Kong.

Fastq files were mapped to the GRCh38 human reference genome using STAR (v2.5.2a) in two-pass mode for the detection of novel splice junctions. Transcript per million (TPM) was quantified using RSEM package in R. Normalized read counts were used for differential expression analysis. Differential expression analysis was carried out using EBSeq and reproduced by DESeq 2 in Bioconductor in R. Principal component analysis (PCA) and pathway analysis were carried out using Partek Genomics Suite 7 (Partek, St Louis, MO, USA). Genes that have a false discovery rate (FDR) of < 0.05 were considered differentially expressed genes. Heatmaps were produced using Morpheus (Broad Institute, Boston, USA). Pathway analysis was done with reference to Kyoto Encyclopedia of Genes and Genomes^{25,26}. Data visualization of differential gene expressions in the form of volcano plots, Venn diagrams, and pathway analysis was carried out using ggplot 2 in R.

Scanning electron microscopy (SEM)

For SEM, U87(lf+) cells were first seeded at 3×10^5 cells per well in a six-well plate. After 24 h to let the cells to adhere to the culture plate, U87(lf+) cells were treated with different drug combinations (PBS, 5 μ M CQ, 1U/ml BCT-100 or 1U/ml BCT-100 + 5 μ M CQ) for 72 h. Cells were then fixed in 2.5% glutaraldehyde at 4 °C overnight. Samples were then dehydrated in a graded series of ethanol, dried using a critical point dryer, and viewed on Hitachi S-3400 Variable Pressure SEM.

Transmission electron microscopy (TEM)

For TEM, U87 or U87(lf+) cells were first seeded at 3×10^5 cells per well in a six-well plate. After 24 h to let the cells to adhere to the culture plate, U87(lf+) cells were treated with different drug combinations (PBS, 5 μ M CQ, 1U/ml BCT-100 or 1U/ml BCT-100 + 5 μ M CQ) for 72 h. U87 were treated with PBS or 1U/ml BCT-100 for 8 h. Then, U87 or U87(lf+) cells were harvested, centrifuged at 300 g for 10 min, and fixed in 2.5% glutaraldehyde at 4 °C overnight. The cell pellets were post-fixed in 1% osmium tetroxide for 1 h at room temperature, dehydrated in ascending grades of ethanol, and embedded in epoxy resin at 60 °C. Ultrathin sections were cut, double stained with uranyl acetate and lead citrate, and viewed on Philips CM100 TEM at an accelerating voltage of 100 kV.

Orthotopic xenograft model and in vivo study

Evaluation of the anti-tumor effect of different drug combinations on U87(lf+) was performed using an orthotopic tumor model, and the study was approved by the Committee on the Use of Live Animals for Teaching and Research (CULATR) of The University of Hong Kong following a previous study²³. All methods were performed in accordance with the relevant guidelines and regulations. Immunocompromised [athymic nude (nu/nu)] mice were purchased from Centre for Comparative Medical Research, the University of Hong Kong. Nude mice of around 20 g at 6 weeks old were anesthetized by the intraperitoneal injection of 50 mg/kg ketamine/xylazine. Mice were fitted onto a stereotactic device for intracranial injections (RWD Life Science Co. Ltd., Shenzhen, China). Briefly, a small skin incision was made to expose the bregma suture, followed by the creation of a small burr hole at anterior–posterior (AP) = +1 and medial–lateral (ML) = −2.5 from bregma by using a micromotor drill (Hager & Meisinger GmbH, Neuss, Germany). A total of 2×10^5 U87(lf+) cells in 5 μ L of PBS were slowly deposited (1 μ L/min) in the right striatum at a depth of −3.5 mm from the dura with a 10 μ L syringe (26-gauge needle; Hamilton Co., Reno, USA). The needle was left in place for 1 min and slowly withdrawn over 3 min followed by the closure of the skin incision with sutures.

For monitoring the tumor progression in the mice with or without drug treatment(s), D-luciferin (Gold Biotechnology, St Louis, USA, LUCK-100, sponsored by Bio-Cancer Treatment Ltd., Hong Kong) was injected into the mice ($n=4$) intraperitoneally (i.p.) after being anesthetized using an intraperitoneal injection of 50 mg/kg of ketamine (Alfasan International, Woerden, Netherlands, 013,004)/xylazine (Alfasan International, Woerden, Netherlands, 013006) every 7 days from the 15th day after tumor engraftment. Group randomization was carried out on the mice showing bioluminescence 15 days after tumor engraftment by throwing a four-sided dice. The mice were treated with PBS, CQ (25 mg/kg in 3 days), BCT-100 (5 mg/kg) or BCT-100 (5 mg/kg) + CQ (25 mg/kg in 3 days), $n=4$. In vivo imaging was detected using a Xenogen IVIS 100. The signal intensity of regions of interest was analyzed by using Living Image® Software (Xenogen Corporation Alameda, USA).

For humane reasons, the mice were euthanized by overdosed ketamine (300 mg/kg)/xylazine (30 mg/kg) i.p. injection if they had a weight loss of $>20\%$ from their baseline weight, showed neurological symptoms, or were in a moribund state due to overdosed isoflurane (Chanelle, UK, IsoVet) inhalation followed by cardiac puncture.

Tissue processing and histology staining

Histopathologic specimens from the mice's brains of in vivo study were harvested after euthanasia, fixed in 10% formaldehyde, and embedded into paraffin blocks. Sections of 4–5 μm in thickness were obtained and stained using hematoxylin and eosin (H&E) and viewed and photographed under Nikon Eclipse Ti2 (Japan). The images were captured and exported as a series of .png files.

Statistical analysis

All the in vitro experiments were performed three times independently with consistent results, " $n=3$ " in the in vitro experiments refers to 3 independent experiments. In XTT assays, the representative data was shown with technical triplicates. Comparisons between the mean values were made using a two-way analysis of variance or unpaired Student *t*-test (one-tailed). The differences were considered statistically significant when $p < 0.05$. For mice survival, Kaplan–Meier analysis was carried out to assess statistical significance. The differences were considered statistically significant when $p < 0.05$ according to the log-rank test.

Results

Arginine auxotrophy found in both the open-source dataset of glioma samples and the glioma cell lines in vitro

The gene expression of OTC and ASS1, were investigated in the open-source dataset mRNA325 from the Chinese Glioma Genome Atlas (<http://www.cgga.org.cn/>). OTC gene expression was absent in all the 85 first-diagnosed GBM samples of various ages (Fig. 1b). All 85 samples expressed ASS1 at a very low level relative to the housekeeping gene GAPDH (Fig. 1b). The OTC and ASS1 protein levels in four glioma cell lines, U87, U373, U138, and D54, were investigated using Western blotting, with mouse liver extract as the positive control. OTC protein expression was absent in all four tested glioma cell lines (Fig. 1ci). ASS1 protein expression was present in the U87 and U138 cell lines but not in the U373 and D54 cell lines (Fig. 1cii). These results suggest that the clinical samples in the open-source dataset and the four glioma cell lines tested may be auxotrophic to arginine.

BCT-100 was cytotoxic to glioma cell lines in vitro

The cellular activities of glioma cell lines under peg-Arg I, BCT-100 treatment, were assessed using XTT assay. The dosages of BCT-100 ranged from 0.3125 U/ml to 10 U/ml. All four glioma cell lines were sensitive to BCT-100 in a dose-dependent manner. The cell viabilities of the U87, U373, and U138 cell lines could be reduced to 50–55% compared to the PBS at the dose of 1.25 U/ml ($p < 0.005$ for all cell lines) after 72 h incubation (Fig. 1di, ii, and iii). The IC_{50} of U87, U373, U138, and D54 were 2.19 ± 0.67 U/ml, 7.82 ± 3.20 U/ml, 0.68 ± 0.12 U/ml, and 0.35 U/ml, respectively (Table 1). At 1.25 U/ml, the cell viability of D54 even was reduced to 30% compared to the PBS ($p < 0.005$ for all cell lines) (Fig. 1div). These results suggested that BCT-100 alone could suppress the cellular activities of all four glioma cell lines tested in vitro.

To test (1) whether BCT-100 was cytostatic or cytotoxic to glioma cell lines and (2) whether citrulline at the serum concentration (40 μM) could rescue glioma cell lines from BCT-100-induced cytotoxicity, AV/PI was used to test the cytotoxicity of the glioma cells treated w/o BCT-100 and/or 40 μM citrulline by using flow cytometry. All four glioma cell lines showed different extents of cell death to BCT-100 treatment, but none of them could be rescued by 40 μM citrulline (Fig. 1ei–iv). These results suggested that BCT-100 could significantly induce cytotoxicity to glioma cell lines in vitro to different extents.

Cell line	IC_{50} (U/ml)
U87	2.19 ± 0.67
U373	7.82 ± 3.20
U138	0.68 ± 0.12
D54	0.38 ± 0.10

Table 1. IC_{50} of glioma cell lines treated with BCT-100 ranged from 0.3125 U/ml to 10 U/ml after 72 h by XTT assay. Result shown is the representative experiment result of triplicates.

Transcriptomic differences of U87 and U373 in response to BCT-100 treatment

The four cell lines treated with BCT-100 showed apparently different extent of cytotoxicity, we performed RNA-seq on U87 and U373 to investigate the possible differences in response to peg-Arg I treatment. Protein-coding mRNA from U87 and U373 treated w/o BCT-100 in three separate independent experiments were used for RNA-seq and data analysis. PCA showed that U87 and U373 formed very distinct clusters, with the first two principal components explaining over 50% of the variance (32.3% for PC1 and 19.3% for PC2; $n = 3$) (Fig. 2a). The differential analysis identified 1,050 up-regulated and 1,225 down-regulated genes for U87 and 883 up-regulated and 846 down-regulated genes for U373 at $FDR < 0.05$, \log_2 fold change $> |1|$, and a minimum mean expression across samples in $TPM > 10$ when the cells were treated w/o 1 U/ml BCT-100 for 72 h, as illustrated by the volcano plots and Venn diagrams (Fig. 2bi, ii, ci, cii). KEGG enrichment pathway analysis also showed that the 10 most significantly changed pathways under BCT-100 treatment in U87 and U373 were partly different (Fig. 2di, ii). The top 10 enriched pathways in U87 were shown in Supplementary Table S1a. The top 10 enriched pathways in U373 were shown in Supplementary Table S1b.

BCT-100-induced autophagy in U87 glioma cells

As BCT-100 is a nutrient-depleting agent, arginine-auxotrophic glioma cells treated with BCT-100 may experience starvation, which may trigger autophagy. The changes in autophagy markers' protein expression and also the cellular structures in the U87 cell line w/o BCT-100 treatment were investigated by harvesting proteins treated with 1 U/ml BCT-100 at different time points (0, 2, 4, and 8 h of treatment). U87 cells treated with 1 U/ml BCT-100 for 8 h showed a significant drop in p62/GAPDH ($p < 0.05$, $n = 3$), and a significant increase in the LC3B-II/I ratio, compared to 0 h of treatment (Fig. 3ai, ii). This suggested that autophagy was significantly induced at 8 h after BCT-100 treatment. Changes in cellular structures in the U87 cells treated w/o 1 U/ml BCT-100 for 8 h were investigated to verify autophagy induction. Autophagosomes (indicated with red arrows) were observed in the U87 cell line using TEM (Fig. 3bi). BCT-100-treated U87 cells showed significantly more autophagosomes than the PBS in 20 random fields ($p < 0.001$, $n = 20$) (Fig. 3bii). These findings suggest that BCT-100 could induce significant autophagy in the U87 cell line at 8 h after treatment.

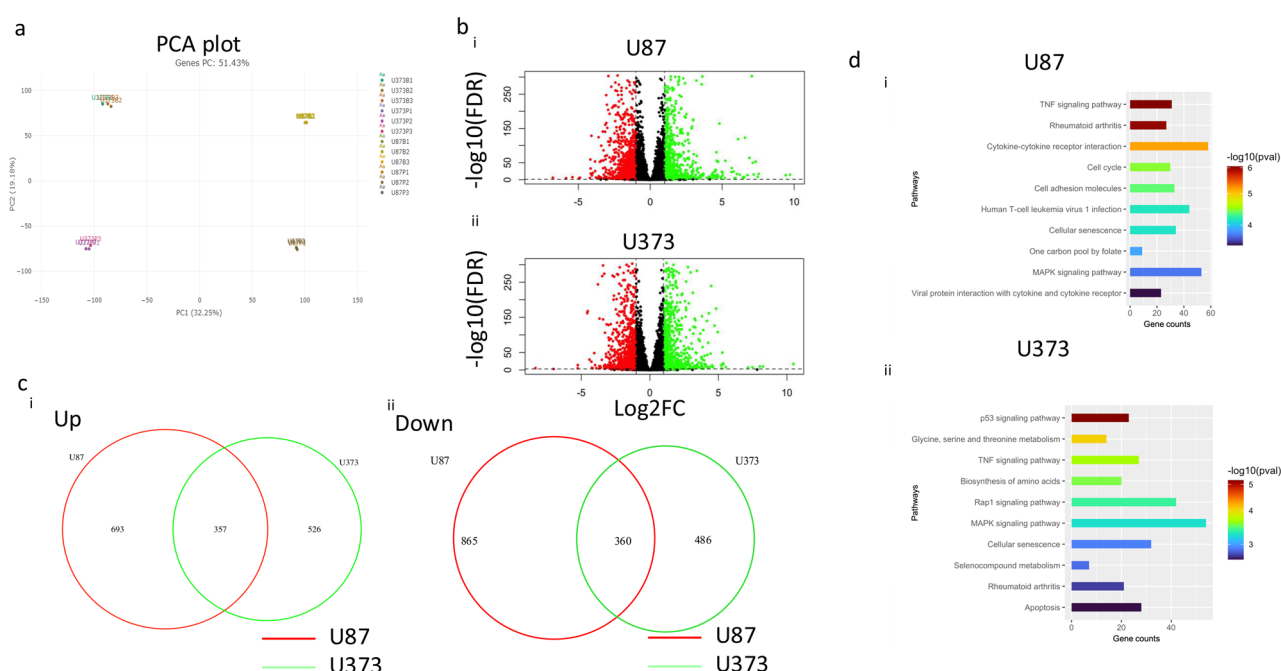


Fig. 2. U87 and U373 responded differently to BCT-100 treatment for 72 h in transcriptomic analysis. (a) Principal component analysis of RNA seq data of the U87 and U373 cell lines treated with or without BCT-100 and visualized as the plot. (b) Volcano plots showing fold changes in gene expression in (i) U87 and (ii) U373 in response to BCT-100 treatment. The green dots refer to significantly up-regulated genes ($FDR < 0.05$, \log_2 (fold changes) > 1 , and mean $TPM > 10$), and the red dots refer to significantly down-regulated genes ($FDR < 0.05$, \log_2 (fold changes) < -1 , and mean $TPM > 10$). The black dots refer to genes of insignificant difference (mean $TPM > 10$) in expression with or without BCT-100 treatment. (c) Venn diagram showing the numbers of differentially expressed genes (DEG) in U87 (as red) and U373 (as green) as (i) up-regulated and (ii) down-regulated genes. (d) KEGG pathway analysis of differentially expressed genes in U87 and U373 in response to BCT-100 treatment. (i) Top 10 KEGG pathway enrichments in U87. (ii) Top 10 KEGG pathway enrichments in U373.

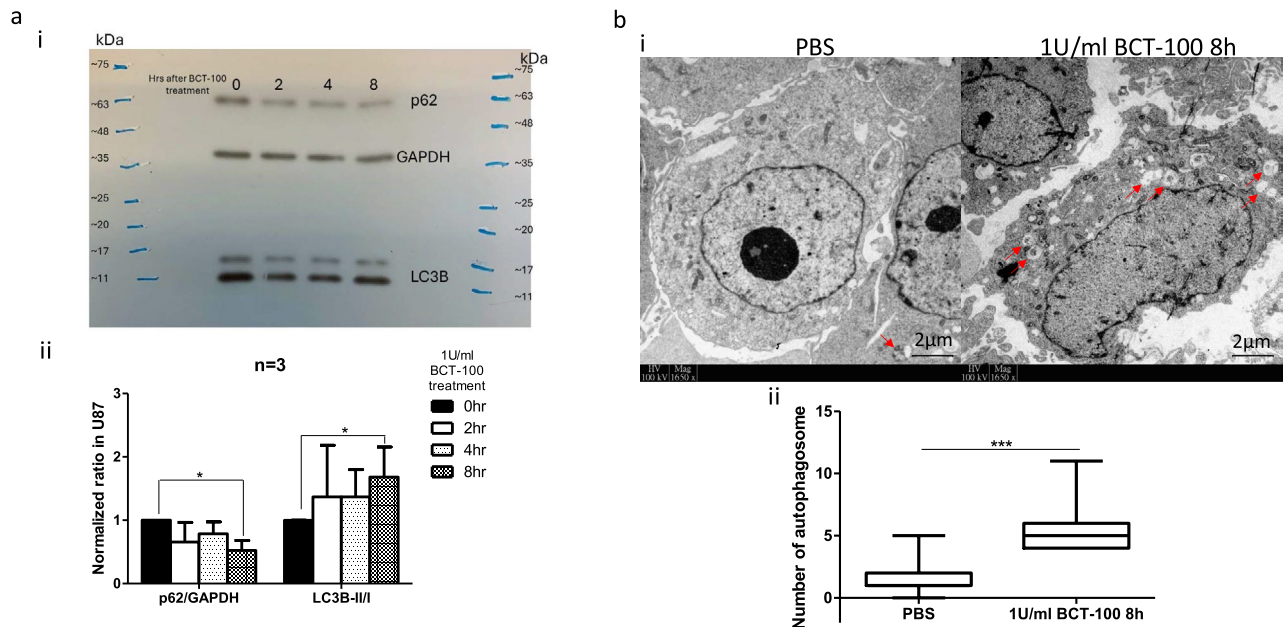


Fig. 3. BCT-100-induced autophagy in U87. **(a) (i)** Western blotting analysis of autophagy markers p62 and LC3B in U87 treated with 1 U/ml BCT-100 for 0, 2, 4, and 8 h. Representative results of three independent experiments are shown. A whole plot is displayed with molecular markers indicating the bands of the corresponding sizes. **(ii)** Quantification of the p62/GAPDH and LC3B-II/LC3B-I ratio of U87 treated with 1 U/ml BCT-100 for 0, 2, 4, and 8 h (n = 3). *: $p < 0.05$ compared between 0 and 8 h. **(b)(i)** TEM image of U87 treated with PBS or 1 U/ml BCT-100 for 8 h. The red arrows indicate the autophagosomes. **(ii)** The quantification of the number of phagosomes observed under TEM in U87 cells treated with PBS or 1 U/ml BCT-100 for 8 h (n = 20). *** $p < 0.001$ between 1 U/ml BCT-100 treated and PBS.

Chloroquine (CQ), but neither TMZ nor DFMO with peg-Arg I, could enhance the cytotoxicity in glioma cell lines

As BCT-100 could induce cell death in vitro in different cell lines, a few drugs were tested as candidates for combined therapy. TMZ, a drug commonly used for glioma treatment, DFMO, a chemical inhibitor of polyamine synthesis in the arginine metabolism pathway, and CQ, an autophagy inhibitor, were tested in combination with BCT-100.

A total of 100 μ M TMZ induced significant cytotoxicity in all four glioma cell lines to a different extent (Fig. 4ai–iv). However, TMZ + BCT-100 did not induce additional cytotoxicity in all four glioma cells, compared to BCT-100 monotherapy (Fig. 4ai–iv). 5 mM DFMO did not induce significant cytotoxicity in all four glioma cell and DFMO + BCT-100 could not induce additional cytotoxicity in all four glioma cell (Fig. 4bi–iv). On the other hand, 5 μ M CQ did not induce significant cytotoxicity in all four glioma cells. However, CQ induced additional increase in the percentage of cell death in all four glioma cells together with BCT-100 treatment to a different extent compared to BCT-100 monotherapy. (U87: $p < 0.05$, U373: $p < 0.01$, U138: $p < 0.01$, D54: $p < 0.01$, n = 3; Fig. 4ci–iv respectively).

Peg-Arg I and CQ induced additive cytotoxicity in U87(lf+) and BCT-100 was caspase-dependent and involved both intrinsic and extrinsic apoptotic pathways

As CQ + BCT-100 induced greater cytotoxicity than BCT-100 alone, we used a luciferase-transfected U87 cell line, U87(lf+), to study the possible mechanisms involved and attempted to use it for the orthotopic glioma model if U87(lf+) showed similar results to Fig. 4ci–iv. Consistent with in vitro responses of other cell lines, BCT-100 induced significant U87(lf+) death over 72 h of treatment ($p < 0.001$, n = 3) and could not be rescued by 40 μ M citrulline (Fig. 5ai).

U87(lf+) also showed enhanced cell death when treated with CQ + BCT-100 compared to BCT-100 alone for 72 h ($p < 0.001$, n = 3) (Fig. 5aii). Unlike the results in Fig. 4ci–iv, in which 5 μ M CQ did not induce significant death in the four cell lines tested, U87(lf+) showed significant U87(lf+) death when treated with 5 μ M CQ ($p < 0.01$, n = 3) (5a(ii)).

To identify the potential mechanism(s) of U87(lf+) death in BCT-100 alone or BCT-100 + CQ, changes in the protein level of caspases 3, 8, and 9 in different treatments for 72 h were investigated. Pan-caspase inhibitor z-vad-fmk was used to test whether CQ + BCT-100 enhanced U87(lf+) cell death in an apoptosis-dependent fashion. 1mM TMZ + z-vad-fmk-treated U87(lf+) showed a significant reduction in cell death compared to 1mM TMZ-treated U87(lf+) alone ($p < 0.001$, n = 3) (Fig. 5aii), suggests that the z-vad-fmk used is functional. Z-vad-fmk-, CQ-, and BCT-100-treated U87(lf+) showed consistent but insignificant reductions in cell death compared to CQ + BCT-100 ($p = 0.1$, n = 3) (Fig. 5aii). BCT-100-treated U87(lf+) showed a significant increase

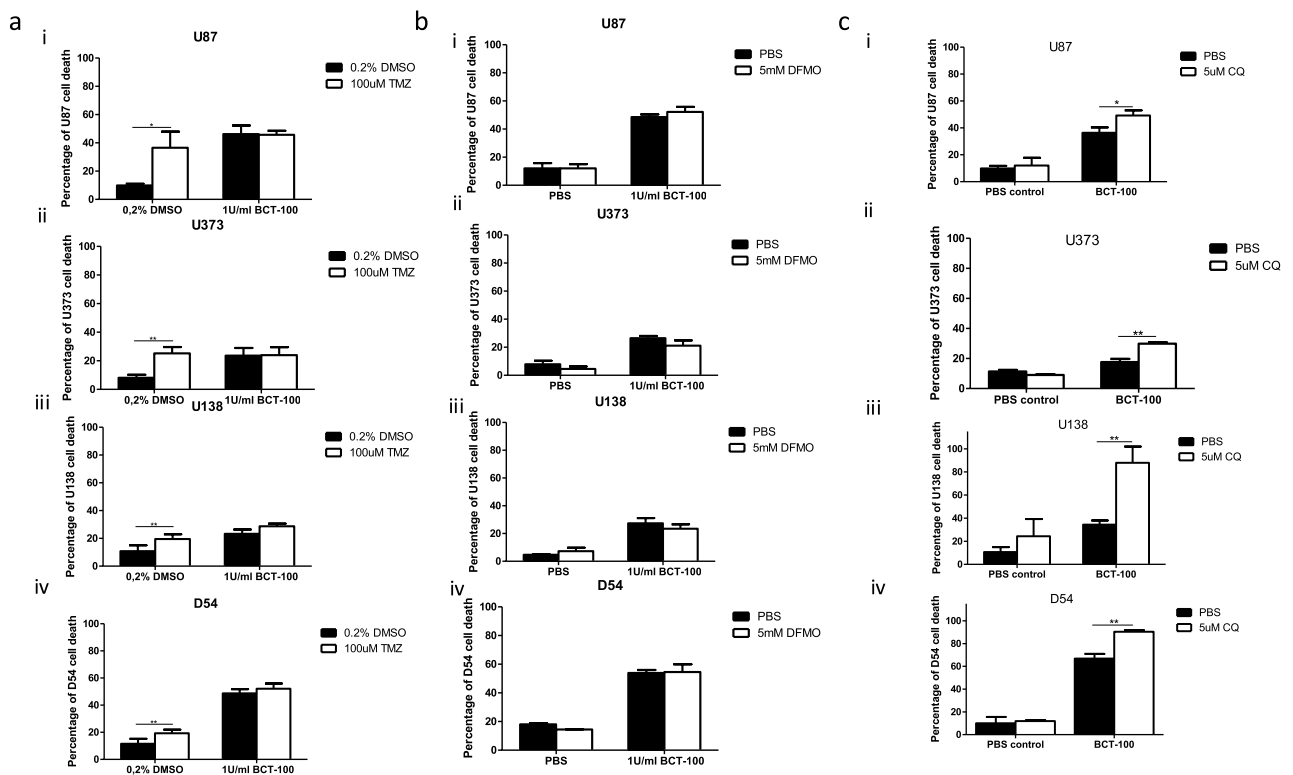


Fig. 4. BCT-100 combined with CQ but not TMZ or DFMO to enhance cytotoxicity. **(a) (i–iv)** The cytotoxicity responses of U87, U373, U138, and D54, respectively, treated with or without 1 U/ml BCT-100 and/or 100 μM TMZ according to annexin V/propidium iodide assay. ** $p < 0.01$ compared between 0.2% DMSO and 100 μM TMZ. * $p < 0.05$ compared between 0.2% DMSO and 100 μM TMZ. **(b) (i–iv)** Cytotoxicity responses of U87, U373, U138, and D54, respectively, treated with or without 1 U/ml BCT-100 and/or 5 mM DFMO, according to annexin V/propidium iodide assay. **(c) (i–iv)** Cytotoxicity responses of U87, U373, U138, and D54, respectively, treated with or without 1 U/ml BCT-100 and/or 5 μM CQ according to annexin V/propidium iodide assay. ** $p < 0.01$ compared between BCT-100 alone and CQ + BCT-100. * $p < 0.05$ compared between BCT-100 alone and CQ + BCT-100.

in active caspase 8 expressing-cell proportion compared to the PBS ($p < 0.05$, $n = 3$), BCT-100 + CQ further increased the active caspase 8-expression ($p < 0.001$, $n = 3$) (Fig. 5a_{iii}). BCT-100-treated U87(lf+) showed a statistically significant slight increase in active caspase 9 expression compared to the PBS ($p < 0.05$, $n = 3$), and BCT-100 + CQ further increased the active caspase 9 expression ($p < 0.001$, $n = 3$) (Fig. 5a_{iv}). CQ showed a significant slight increase in active caspase 3 expression compared to the PBS ($p < 0.01$, $n = 3$), and BCT-100-treated U87(lf+) showed a significant increase in active caspase 3 expression compared to the PBS ($p < 0.001$; $n = 3$). BCT-100 + CQ further increased the active caspase 3 expression ($p < 0.001$; $n = 3$) (Fig. 5a_v). Although z-vad-fmk did not significantly rescue CQ + BCT-100-treated U87(lf+), the up-regulation of active caspases 3, 8, and 9 in BCT-100-treated and CQ + BCT-100-treated U87(lf+) suggested that BCT-100-induced cell death involves both extrinsic and intrinsic apoptotic pathways and could be further enhanced by CQ.

When we investigated the cell membrane morphology and subcellular structures of U87(lf+) under different treatments, obvious structural changes were observed. When using SEM, no obvious surface changes were observed in U87(lf+) treated with BCT-100 and/or CQ (Fig. 5b_{i–iv}).

Peg-Arg I prolonged the survival of intracranial U87(lf+)-engrafted mice; however, CQ + peg-Arg I did not further prolong the survival of glioma mice

As CQ + BCT-100 treatment demonstrated significant cell-death induction in different glioma cell lines, the studies were extended to investigate survival in vivo. U87(lf+) cells were injected intracranially into nude mice, as described previously, and tumor growth was evaluated by using quantitative bioluminescence imaging every 7 days. Bioluminescence was first detected on day 15 after the intracranial injection of U87(lf+), and, at this point, the animals were randomly assigned into two groups of four animals and treated with PBS or BCT-100 monotherapy at 10 mg/kg every 3 days, $n = 4$ (Fig. 6a_i). Drug treatments started on day 16 after the injection of U87(lf+). An increase in bioluminescence was observed in both groups (Fig. 6a_{ii}). The median survival of the PBS and BCT-100-treated mice were 30 and 34 days, respectively ($p < 0.05$, $n = 4$) (Fig. 6a_{iii}). The U87(lf+)-injected mice experienced sudden weight loss upon deteriorated health under PBS or BCT-100 treatment, and BCT-100 treatment did not cause significantly further weight loss in the mice (Fig. 6a_{iv}). Such weight loss is unlikely to be due to BCT-100 treatment, as nude mice without tumor burden did not show any weight loss after

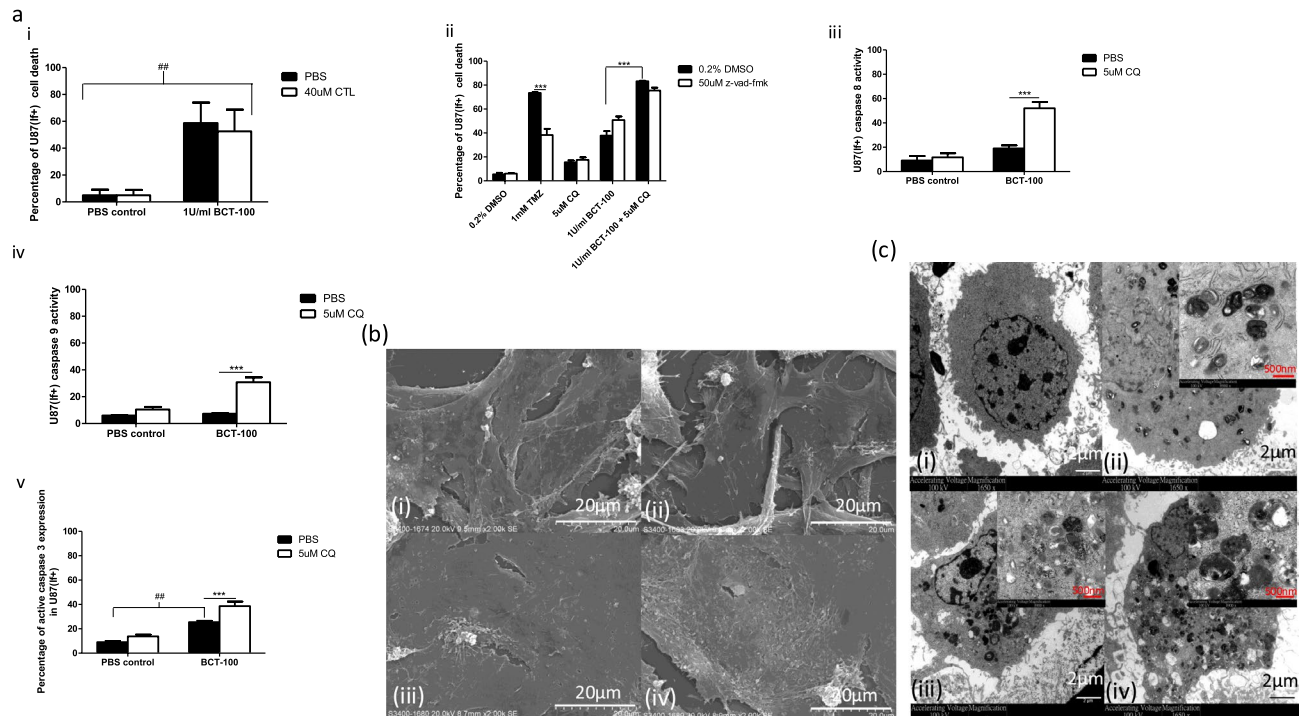


Fig. 5. BCT-100 + CQ induced caspase-dependent and caspase-independent cell death in U87(lf+). **(a)(i)** Cytotoxicity response of U87(lf+) treated with or without 1 U/ml BCT-100 and/or 40 μM citrulline for 72 h determined by using annexin V/propidium iodide assay. $##p < 0.01$ compared between PBS groups and 1 U/ml BCT-100 groups. **(ii)** Cytotoxicity response of U87(lf+) treated with or without 1 mM TMZ, 5 μM CQ, 1 U/ml BCT-100, or pan-caspase inhibitor 50 μM z-vad-fmk for 72 h determined by using annexin V/propidium iodide assay. $***p < 0.001$ between groups compared, respectively. **(iii)** Caspase 8 activity of U87(lf+) treated with or without 5 μM CQ or 1 U/ml BCT-100 for 72 h determined by flow cytometry. $***p < 0.001$ compared between BCT-100 alone and BCT-100 + CQ-treated U87(lf+). **(iv)** Caspase 9 activity of U87(lf+) treated with or without 5 μM CQ or 1 U/ml BCT-100 for 72 h determined by using flow cytometry. $***p < 0.001$ compared between BCT-100 alone and BCT-100 + CQ-treated U87(lf+). **(v)** Caspase 3 activity of U87(lf+) treated with or without 5 μM CQ or 1 U/ml BCT-100 for 72 h determined by using flow cytometry. $##p < 0.01$ compared between the PBS and CQ. $***p < 0.001$ compared between BCT-100 alone and BCT-100 + CQ-treated U87(lf+). **(b)** and **(c)** show changes in the cellular surface and subcellular substructures in BCT-100- and/or CQ-treated U87(lf+) after 72 h. **(b)** Scanning electron microscopy pictures of U87(lf+) in **(i)** PBS, **(ii)** 5 μM CQ, **(iii)** 1 U/ml BCT-100, and **(iv)** BCT-100 + CQ for 72 h. **(c)** Transmission electron microscopy pictures of U87(lf+) in **(i)** PBS, **(ii)** 5 μM CQ, **(iii)** 1 U/ml BCT-100, and **(iv)** BCT-100 + CQ for 72 h.

being treated with 10 mg/kg BCT-100 every 3 days for 28 days (Supplementary Fig. S2; $n = 4$). Nevertheless, BCT-100 treatment prolonged the survival of U87(lf+)-engrafted mice, and therefore, further studies of a combination of CQ + BCT-100 were undertaken.

The combination therapy dosages of BCT-100 and CQ involved cycles of 10 mg/kg of BCT-100 every 3 days and 25 mg/kg of CQ over 3 days (15 mg/kg CQ on the first day and 5 mg/kg CQ on the second and third day, using malaria treatment dosages as a reference) simultaneously^{27,28} (Fig. 6bi1). The dosage was first tested in mice without tumors. Significant weight reduction was observed in the mice treated with combination therapy after 5 days, suggesting the possibility of toxicity and, therefore, the experiment of combination therapy stopped (Supplementary Fig. S3; $n = 3$). Therefore, the BCT-100 dosage in the combination therapy was reduced to 5 mg/kg every 3 days and tested again in nude mice without tumors. It was found that, after 14 days of treatment, the mice treated with different drugs did not show any significant changes in body weight, suggesting this dosage was safe for treating U87(lf+)-inoculated mice (Supplementary Fig. S4; $n = 4$).

Then, an animal study using another batch of intracranial glioma-bearing mice was performed in four groups with four mice each by using the following cycles of treatments: PBS, 25 mg/kg CQ in 3 days, 5 mg/kg BCT-100 monotherapy every 3 days, and a combination therapy of CQ and BCT-100 using the same dosages as the monotherapy groups ($n = 4$) (Fig. 6b(i)1 and 2). Tumor growth was also evaluated by using quantitative bioluminescence imaging every 7 days. Bioluminescence was first detected on day 15 after the intracranial inoculation of U87(lf+), and at this point, the animals were randomly assigned into four groups of four animals each and treated as described above. Drug treatments were started on day 16 after implanting U87(lf+). An increase in bioluminescence was observed in both groups (Fig. 6bii). The median survival of the PBS, CQ, BCT-100, and CQ + BCT-100 were 31.5, 42.5 ($p < 0.05$ vs PBS, $n = 4$), 35.5 ($p < 0.05$ vs PBS, $n = 4$), and 35 ($p = 0.101$ vs PBS, $n = 4$) days, respectively (Fig. 6biii). The U87(lf+)-inoculated mice experienced gradual and/or sudden

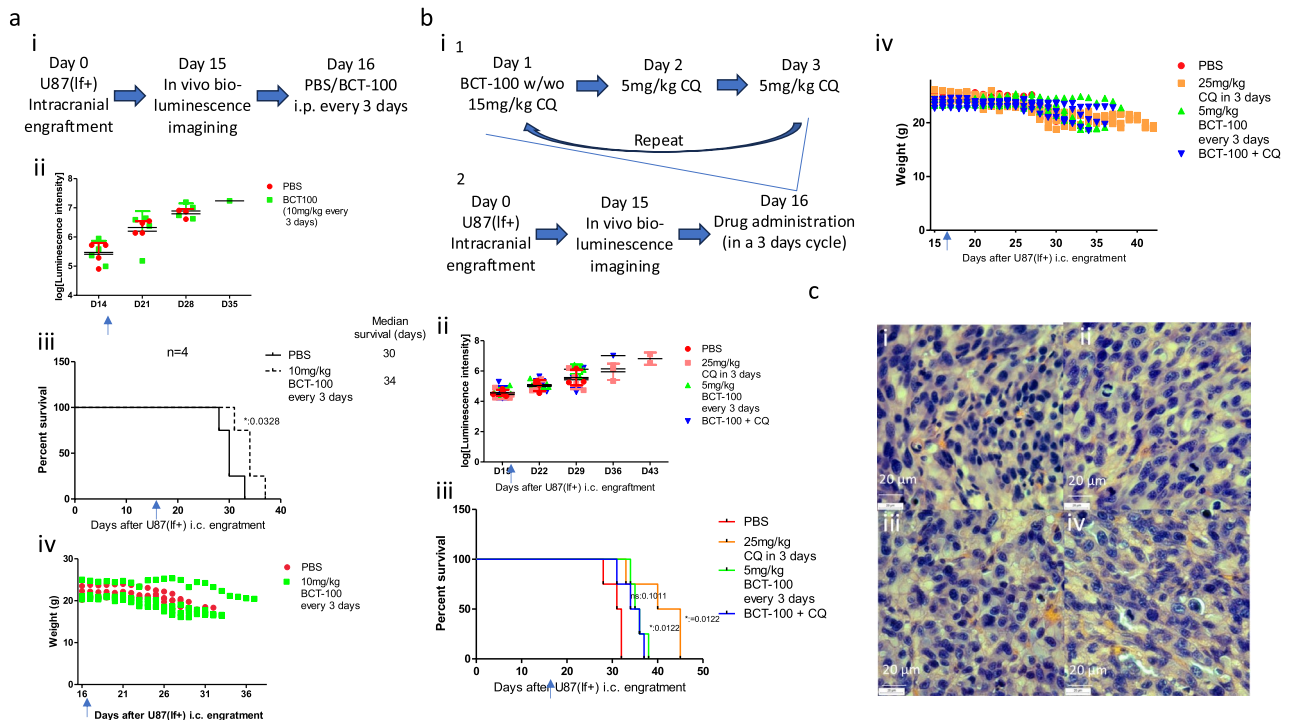


Fig. 6. BCT-100 or CQ alone prolonged intracranial U87(lf+)-bearing mice's survival; no further enhancement in the CQ + BCT-100 group. **(a)** **(i)** Gradual increase in bioluminescence intensity of intracranial U87(lf+)-bearing mice expressed in log(bioluminescence intensity) with or without i.p. injection of 10 mg/kg BCT-100 every three days ($n = 4$). The arrow indicates the day of starting the BCT-100 injection. **(ii)** Kaplan–Meier survival curves of U87(lf+)-bearing mice defined by mice showing a weight drop of more than 20% before drug treatment was started, neurological symptoms found, or moribund state. The arrow indicates the starting day of the BCT-100 injection. Prolonged survival was observed in the BCT-100-treated group ($n = 4$) * $p < 0.05$ compared to the PBS group. **(iii)** Gradual weight drop of U87(lf+)-bearing mice from the day of starting BCT-100 injection to death ($n = 4$). The arrow indicates the starting day of the BCT-100 injection. **(b)** **(i)** Bioluminescence intensity of intracranial U87(lf+)-bearing mice expressed in log(bioluminescence intensity) with or without i.p. injection of 25 mg/kg CQ every three days and/or 10 mg/kg BCT-100 every three days ($n = 4$). The arrow indicates the day of starting the BCT-100 injection. A gradual increase in bioluminescence was observed in all groups. **(ii)** Kaplan–Meier survival curves of U87(lf+)-bearing mice defined by mice showing a weight drop of more than 20% before drug treatment was started, neurological symptoms found, or moribund state. The arrow indicates the day of starting BCT-100 and/or CQ injection. Prolonged survival was observed in CQ- or BCT-100-treated groups but not in the combined therapy group ($n = 4$). * $p < 0.05$ compared to the PBS group. **(iii)** Gradual weight drop of U87(lf+)-bearing mice from the day of starting BCT-100 and/or CQ injection to death ($n = 4$). The arrow indicates the day of starting the BCT-100 injection. **(c)** H&E staining of xenografts from mice developed from U87(lf+) treated with **(i)** PBS, **(ii)** 25 mg/kg CQ every three days, **(iii)** 5 mg/kg BCT-100 every three days, or **(iv)** combined BCT-100 and CQ therapy (600 \times). No obvious changes were observed between the different treatment groups.

weight loss before being euthanized (Fig. 6aiv). No obvious changes in tumor cell density were observed in the H&E tissue section slides of the drug-treated groups compared to the PBS (Fig. 6ci–iv). In summary, CQ treatment and BCT-100 treatment but not combinational therapy significantly prolonged the survival of U87(lf+)-engrafted mice, and therefore, further investigation was carried out in attempt to explain the reason(s) behind the differences between the in vitro and in vivo results.

Mouse microglia cell line BV2 protected U87(lf+) from peg-Arg I treatment in Transwell co-culture; this protective effect was partly used to induce cytotoxicity in BV2 cells before Transwell co-culture

As BCT-100 did not induce significant cytotoxicity in the orthotopic glioma mouse model, as in the in vitro results, there is a possibility that the presence of certain factor(s) in the tumor microenvironment may be the reason(s) behind this. Microglia, an important component in the glioma microenvironment, was tested for its possibility to confer protection to glioma cells against BCT-100 treatment. The mouse microglia cell line BV2, pretreated with mouse IFN- γ or IL-4 for 48 h, was immunophenotyped by using flow cytometry using the M1 and M2 polarization markers CD86 and CD206, respectively. Mouse IFN- γ - or IL-4-treated BV2 showed significantly up-regulated CD86 ($p < 0.05$, $n = 3$) and CD206 ($p < 0.05$, $n = 3$), respectively, suggesting BV2 cells might be polarized to M1 or M2 upon exposure to IFN- γ or IL-4 (Fig. 7a). M0- (unpolarized state), M1-, or

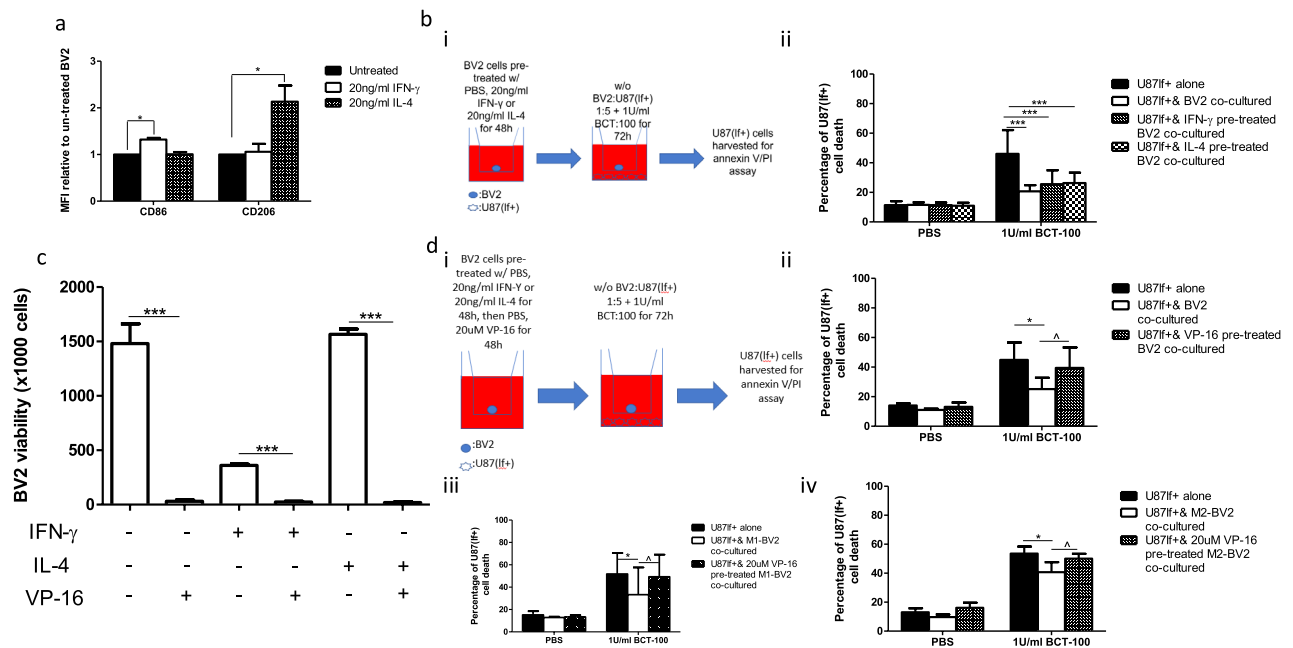


Fig. 7. Transwell-co-cultured BV2 cells protected U87(lf+) against BCT-100; pretreating BV2 with etoposide suppressed such protection. **(a)** The immunophenotyping of BV2 cells treated with or without mouse IFN- γ or mouse IL-4 for 48 h. * $p < 0.05$ between groups were compared. **(b) (i)** Schematic diagrams of experimental setup. **(ii)** Cytotoxicity responses of U87(lf+) with or without different cytokine-pretreated BV2 transwell co-culture and treated with or without 1 U/ml BCT-100 for 72 h determined by using annexin V/propidium iodide assay. *** $p < 0.001$ compared between U87(lf+) in M0-, M1-, or M2-polarized BV2 Transwell co-culture and U87(lf+) alone (i.e., not co-cultured with BV2). **(c)** Trypan blue exclusion assay of BV2 cells treated with PBS or 20 μ M etoposide. ***number of viable BV2 treated with 20 μ M VP-16 compared to PBS. **(d) (i)** Schematic diagrams of the experimental setup. **(ii-iv)** Cytotoxicity responses of U87(lf+) with or without VP-16 pretreated BV2 Transwell co-culture and treated with or without 1 U/ml BCT-100 for 72 h determined by using annexin V/propidium iodide assay. * $p < 0.05$ compared between U87(lf+) in BV2 Transwell co-culture and U87(lf+) alone. ^ $p < 0.05$ compared between U87(lf+) in BV2 Transwell co-culture pretreated with or without VP-16.

M2-polarized BV2 cells were co-cultured in a transwell with U87(lf+) and treated with BCT-100 for 72 h. The experimental setup is illustrated in Fig. 7b(i). BV2 significantly reduced the cell death of U87(lf+) during BCT-100 treatment ($p < 0.001$, $n = 3$), regardless of the microglial polarization state of BV2 (Fig. 7b(ii)). Such results suggest that BV2 could protect U87(lf+) against BCT-100-induced cell death by using species nonspecific soluble factor(s). In order to suppress BV2, VP-16 (etoposide) was tested to determine whether it can induce cytotoxicity in BV2 upon 48 h of treatment. By using trypan blue exclusion, M0-, M1-, and M2-polarized VP-16-treated BV2 showed a significant reduction in number of viable cells ($p < 0.001$, $n = 3$) (Fig. 7c). Such a result suggested that VP-16 could suppress cell growth and induce cell death in BV2 in unpolarized, M1, and M2 polarization states. Based on such findings, BV2 cells were pretreated with VP-16 for 48 h before Transwell co-culture with U87(lf+). The experimental setup is illustrated in Fig. 7d(i). VP-16-pretreated BV2, no matter what polarization state (M0, M1, or M2), had a decreased protective effect on U87(lf+) from BCT-100-induced cell death. A significant difference can be demonstrated by comparing U87(lf+) with un-treated M0, M1, or M2 BV2 transwell co-culture vs. U87(lf+) with VP-16-pretreated M0, M1, or M2 BV2 transwell co-culture ($p < 0.05$; $n = 3$) (Fig. 7dii-iv). Such results suggest that VP-16 could partly suppress the protection of BV2 to U87(lf+) against BCT-100-induced cell death.

Discussion

Arginine is known to be an important nutrient for cancer growth, survival and proliferation¹⁷. In tumor micro-environment, arginine is a tumor-promoting metabolite²⁹. Arginine may help maintaining the microenvironment to be pro-cancer and immunosuppressive by stimulating non-cancer cells in the microenvironment to deplete nutrients (including arginine) and accumulate immunosuppressive metabolites⁴. Cancer cells have either low or absent urea cycle enzyme gene expression and they count on exogenous arginine as nutrient by up-regulating arginine transporters to compete nutrients with surrounding non-cancer cells³⁰. Therefore, arginine deprivation approach may suppress growth or even induce cancer cell death. Considering both the arginine auxotrophy in cancer cells and the pro-cancer nature of arginine in tumor micro-environment, arginine deprivation becomes a novel approach as cancer therapy under investigation. There have been numerous studies on arginine depletion-based therapy exploiting the arginine auxotrophy in different cancers, e.g. lung cancer, breast cancer, pancreatic

cancer, melanoma and leukemia³¹. In general, our study of BCT-100 showed significant cytostatic and cytotoxic effects on GBM cell lines in vitro. However, variations in response do exist. U373 and U138 cell lines showed apparently less cell death compared to U87 and D54 after BCT-100 treatment. Consistently with other cancers' in vitro findings, BCT-100 suppressed growth and induced cell death in GBM cell lines⁶. The different extent of cell death in different GBM cells we found also suggest that factors other than OTC and ASS1 expressions may affect the cancer cells' arginine depletion therapy response.

From transcriptomic analysis of the U87 and U373, we found that U87 and U373 cell lines responded differently, as illustrated in PCA (Fig. 2a). U87 was known to have wild-type TP53, and U373 was known to have mutant TP53. We found that, in our cell lines, both U87 and U373 carry a non-pathogenic homozygous TP53 mutation, P72R, but U373 has the pathogenic hotspot TP53 R273H homozygous mutation (Supplementary Fig. S5)^{32,33}. Pathogenic TP53 mutation may give a hint about the resistant mechanism(s) to BCT-100 treatment, and the role of TP53 mutation in peg-Arg I treatment response should be further investigated. On the other hand, p53 signaling mRNA expression data in both U87 and U373 showed one pro-apoptotic receptor, death receptor 5 (DR5) to be significantly up-regulated after BCT-100 treatment (Supplementary Figs. S7a,b and S7a,b). A similar finding has been reported in another RNAseq dataset, GSE104105, based on an in vitro study of breast cancer cell line MDA-MB231. Arginine-starved MDA-MB231 showed significantly up-regulated DR4 gene expression (Supplementary Fig. S7c)³⁴. DR4 and DR5 are tumor necrosis factor-associated ligand-inducing apoptosis (TRAIL) receptors³⁵. Both DR4 and DR5 may induce apoptosis by TRAIL activation, and they are expressed in different types of cancer³⁵. Our RNAseq data may provide insight into drug combination design of arginine depletion with death receptor agonists under clinical trials for cancer treatment³⁶. Further investigations may help identifying the regulatory mechanisms of DR4 and DR5 expressions, as the differences in response were noted in the reported breast cancer cell line and our GBM cell lines.

BCT-100-induced autophagy is like other arginine-depletion enzymes such as peg-ADI and modified human peg-Arg I^{22,37}. In a study of an intracranial U87-engraftment mouse model, TMZ and peg-ADI caused significantly reduced tumor growth compared to peg-ADI monotherapy²¹. In our in vitro study, TMZ + BCT-100 did not show enhanced cell death compared to the monotherapies of TMZ and BCT-100 (Figs. 4ai–iv). In a study using a subcutaneous mouse model of different lung adenocarcinoma cell lines, a polyamine synthesis pathway inhibitor, DFMO, caused significantly reduced tumor growth and induced apoptosis compared to BCT-100 monotherapy³⁸. In our in vitro study, TMZ + BCT-100 did not enhance cell death compared to the monotherapies of either TMZ or BCT-100 (Figs. 4ai–iv). Our findings did not necessarily contradict others' results. The synergistic growth suppression by peg-ADI + TMZ in the intracranial U87-engraftment mouse model suggested that such a combination may be an effective cytostatic therapy but may not necessarily induce synergistic cytotoxicity in GBM tissues²¹. The synergistic cytotoxicity of DFMO and BCT-100 may be cancer-type dependent. Nonetheless, an orthotopic tumor animal model should be required to estimate the therapeutic efficacies of different treatments. Consistent with findings from other tumor models in vitro using arginine depletion-based therapy, CQ at a nonlethal dose enhanced cytotoxicity in all the glioma cell lines compared to BCT-100 monotherapy (Fig. 4ci–iv)^{37,39–41}. Mechanistic studies of such phenomena may provide a better understanding of how to maximize the cytotoxic effect of CQ + arginine depletion-based therapy, and an orthotopic GBM mouse model will be required to verify the in vitro findings.

In our results, BCT-100 activated caspases 3 and 8 levels, and CQ + BCT-100 enhanced activated caspase 3, 8, and 9 levels (Fig. 5aiii–v). Such findings suggest that BCT-100 may induce U87(lf+) apoptosis via an extrinsic pathway, and CQ + BCT-100 may further induce apoptosis via an intrinsic pathway in addition to an extrinsic pathway when using BCT-100 alone. When pan-caspase inhibitor z-vad-fmk was used to verify whether BCT-100- and CQ + BCT-100-induced cell death are caspase-dependent, unexpected results were encountered. Paradoxically, z-vad-fmk + BCT-100 induced even more U87(lf+) death than BCT-100 alone, suggesting such a combination would facilitate caspase-independent cell death (Fig. 5aii). Some studies have shown that z-vad-fmk could induce non-apoptotic cell death in mouse macrophages and fibroblasts in vitro^{42,43}. z-vad-fmk reduced CQ + BCT-100-treated U87(lf+) death significantly, but not to a huge extent (Fig. 5aii). By observing the cellular structural changes in U87(lf+) treated with CQ + BCT-100 by using SEM, pores were observed in the cell membrane, which was not a feature of apoptosis (Fig. 5biv)⁴⁴. All these findings suggest that BCT-100 monotherapy and CQ + BCT-100 may induce both caspase-dependent and caspase-independent cell death. Similar findings were also reported in a study using another arginine depleting agent, ADI-PEG20 in glioblastoma which caused caspase-independent cell death⁴⁵.

We used an intracranial GBM mouse model to verify the in vitro findings that BCT-100 induces cell death, which can be further enhanced by CQ. Therefore, we used cycles of BCT-100 and CQ treatment on the GBM-bearing mice. The survival of the mice was significantly prolonged by BCT-100 treatment alone. However, the CQ + BCT-100 combination did not further prolong mice survival (Fig. 6b(ii)). Interestingly, CQ could significantly prolong the survival of GBM-bearing mice without causing tumor shrinkage (Figs. 6bi, ii). The prolonged survival in CQ-treated GBM-bearing mice may be due to the intracellular accumulation of CQ over time, and the long CQ half-life may induce cytotoxicity slowly and gradually⁴⁶. However, it is uncertain whether the CQ dose we used, which is based on anti-malaria dosage, was optimal for GBM treatments, as there have been pre-clinical studies that used higher CQ doses with significant anti-cancer effects^{47,48}. Therefore, a higher CQ dose may have a more significant anti-tumor effect in combination with BCT-100 in GBM in vivo despite a higher risk of toxicity. Nonetheless, the in vivo findings showed significant differences compared to the in vitro findings, and further investigation is needed to figure out the mechanisms causing these differences.

As we hypothesized, the discrepancies between our in vitro and in vivo results may be due to protection mechanisms conferred by other cells within the tumor microenvironment. Therefore, we tested microglia/GBM interaction. This is because microglia may account for up to 30% of the tumor microenvironment, suggesting it may play a significant role in GBM survival^{49,50}. We used the BV2 microglia cell line for the microglia/

GBM Transwell co-culture as BV2 is a mouse microglia cell line that may resemble the microglia of tumor microenvironment in the intracranial GBM mouse model⁵¹. Our Transwell co-culture study showed that BV2 could provide species nonspecific protection to U87(lf+) via soluble factor(s), regardless of the BV2 M1 or M2 polarization state (Fig. 6bii). Such a result is similar to our previous findings, in which human mesenchymal stromal cells (hMSCs) could significantly protect BCT-100-treated human leukemic cell lines from cell death in Transwell co-culture²⁴. Such protection could be suppressed by pretreating the hMSCs with vincristine, a microtubule-disrupting chemotherapeutic agent that could induce hMSC cell death⁵². We used a similar strategy towards BV2/U87(lf+) Transwell co-culture in this study by pretreating the BV2 cells with etoposide before co-culturing with U87(lf+) in an attempt to suppress microglial support. Such a design was based on the hypothesis that, if etoposide is cytotoxic to peripheral blood monocytes, it may also suppress macrophages, which are derived from monocytes⁵³. Our results showed that etoposide could induce cell death and suppress the growth of BV2; etoposide pretreated BV2 also showed significantly reduced protection to U87(lf+) against BCT-100 treatment (Fig. 7dii–iv). To the best of our knowledge, this is the first report showing the protective effect of microglial cells on GBM cells during arginine-deprivation therapy, while there have been some studies that address the microglia-conferred chemoresistance in GBM cells during other therapies⁵⁴. Such findings suggest the use of combination therapy by suppressing the GBM-supporting niche before arginine deprivation therapy. On the other hand, a recent report shows that the combination of irradiation and peg-ADI activates the anti-tumor phenotype of glioma-associated macrophages/microglia *in vivo* and could eradicate intracranial mouse GBM and prolong mice survival by enhancing cytotoxic peroxynitrite production and promoting the polarization of GBM-associated microglia/macrophages into an anti-tumor type²⁰. It also showed that combining irradiation and peg-ADI treatment induced BV2 microglial cells into a pro-inflammatory phenotype²⁰. Such findings imply arginine deprivation, together with irradiation, may turn the microglia in the GBM microenvironment from a pro-tumor to an anti-tumor phenotype²⁰. Our findings and the recently reported findings suggest that modulating the microglial polarization or suppressing the microglia niche may enhance the efficacy of arginine deprivation therapy for clinical use. In the future, the change(s) in immune status of tumor microenvironment of GBM cells treated with other arginase I-based combination therapy will be investigated. This is to investigate the potential of arginase I-based therapy in turning pro-tumor microenvironment into an anti-tumor microenvironment for tumor suppression. A graphic scheme integrating the results obtained is illustrated in Fig. 8.

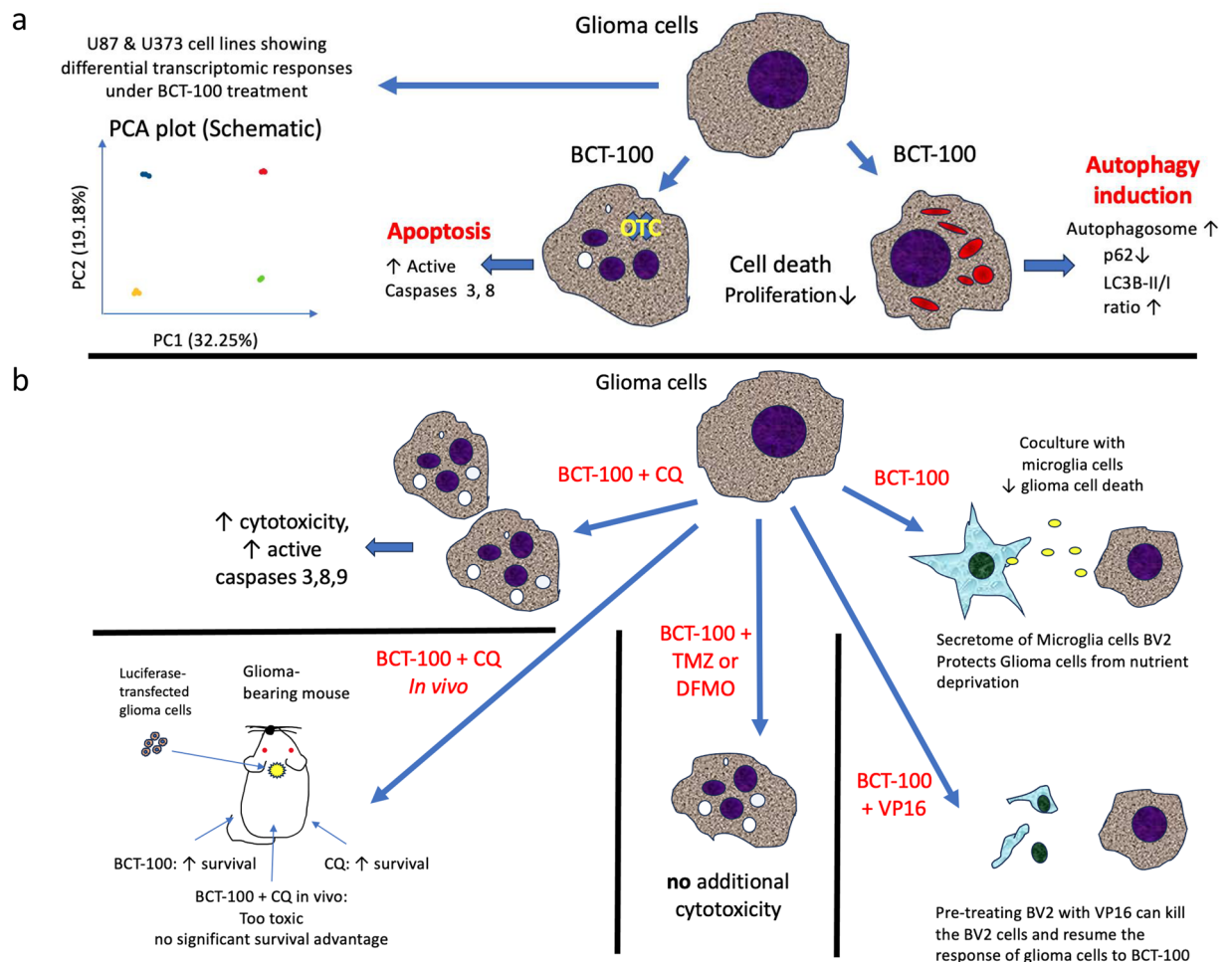


Fig. 8. The graphic scheme summarizing all the research findings. **(a)** Glioma cells are found arginine-auxotrophic with no OTC expression. BCT-100 suppressed proliferation and induced cell death in glioma cell lines. Transcriptomic analysis showed differential gene expression patterns in U87 and U373 glioma cell lines treated with BCT-100 as shown in principal component analysis (schematic PCA shown). BCT-100 induced autophagy and active caspases 3, 8 expressions in glioma cells. **(b)** BCT + chloroquine (CQ) showed enhanced glioma cytotoxicity compared to BCT-100 with active caspase 9 expression and enhanced caspases 3, 8 expression. Such enhanced cytotoxicity was not observed in glioma cells treated with BCT-100 + temozolomide nor difluoromethylornithine. BCT-100 and CQ but not BCT-100 + CQ prolonged survival of mice engrafted with luciferase-transfected glioma cells intracranially. Microglia cells BV2 protected glioma cells from BCT-100 induced cytotoxicity. Etoposide (VP-16) pre-treatment on BV2 suppressed its protection to glioma cells against BCT-100, making glioma cells vulnerable to BCT-100-induced cytotoxicity.

Data availability

RNA-seq data were deposited into the NCBI GEO database and are available under accession number GSE233759 from this link <https://www.ncbi.nlm.nih.gov/geo/query/acc.cgi?acc=GSE233759>. The data analyzed in this study are available from the corresponding author, Prof. G.C.F Chan, upon reasonable request.

Received: 10 March 2025; Accepted: 28 July 2025

Published online: 08 August 2025

References

- Rong, L., Li, N. & Zhang, Z. Emerging therapies for glioblastoma: current state and future directions. *J. Exp. Clin. Cancer Res.* **41**, 142. <https://doi.org/10.1186/s13046-022-02349-7> (2022).
- Hanif, F., Muzaffar, K., Perveen, K., Malhi, S. M. & Simjee, S. U. Glioblastoma Multiforme: A review of its epidemiology and pathogenesis through clinical presentation and treatment. *Asian Pac. J. Cancer Prev.* **18**, 3–9. <https://doi.org/10.22034/APJCP.2017.18.1.3> (2017).
- Angom, R. S., Nakka, N. M. R. & Bhattacharya, S. Advances in glioblastoma therapy: An update on current approaches. *Brain Sci.* <https://doi.org/10.3390/brainsci13111536> (2023).
- Albaugh, V. L., Pinzon-Guzman, C. & Barbul, A. Arginine-Dual roles as an onconutrient and immunonutrient. *J. Surg. Oncol.* **115**, 273–280. <https://doi.org/10.1002/jso.24490> (2017).

5. Patil, M. D., Bhaumik, J., Babykutty, S., Banerjee, U. C. & Fukumura, D. Arginine dependence of tumor cells: Targeting a chink in cancer's armor. *Oncogene* **35**, 4957–4972. <https://doi.org/10.1038/onc.2016.37> (2016).
6. Fung, M. K. L. & Chan, G. C. Drug-induced amino acid deprivation as strategy for cancer therapy. *J Hematol Oncol* **10**, 144. <https://doi.org/10.1186/s13045-017-0509-9> (2017).
7. Vardon, A. et al. Arginine auxotrophic gene signature in paediatric sarcomas and brain tumours provides a viable target for arginine depletion therapies. *Oncotarget* **8**, 63506–63517. <https://doi.org/10.18632/oncotarget.18843> (2017).
8. Riess, C. et al. Implementation of a combined CDK inhibition and arginine-deprivation approach to target arginine-auxotrophic glioblastoma multiforme cells. *Cell Death Dis.* **13**, 555. <https://doi.org/10.1038/s41419-022-05006-1> (2022).
9. Chung, S. F. et al. Mono-PEGylated thermostable *Bacillus caldovelox* arginase mutant (BCA-M-PEG20) induces apoptosis, autophagy, cell cycle arrest and growth inhibition in gastric cancer cells. *Invest New Drugs* **40**, 895–904. <https://doi.org/10.1007/s10637-022-01265-z> (2022).
10. Stone, E. M. et al. Replacing Mn(2+) with Co(2+) in human arginase i enhances cytotoxicity toward l-arginine auxotrophic cancer cell lines. *ACS Chem. Biol.* **5**, 333–342. <https://doi.org/10.1021/cb900267j> (2010).
11. Al-Koussa, H., El Mais, N., Maalouf, H., Abi-Habib, R. & El-Sibai, M. Arginine deprivation: A potential therapeutic for cancer cell metastasis? A review. *Cancer Cell Int.* **20**, 150. <https://doi.org/10.1186/s12935-020-01232-9> (2020).
12. Field, G. C., Pavlyk, I. & Szlosarek, P. W. Bench-to-bedside studies of arginine deprivation in cancer. *Molecules* <https://doi.org/10.3390/molecules28052150> (2023).
13. Butler, M., van der Meer, L. T. & van Leeuwen, F. N. Amino acid depletion therapies: Starving cancer cells to death. *Trends Endocrinol Metab* **32**, 367–381. <https://doi.org/10.1016/j.tem.2021.03.003> (2021).
14. Yau, T. et al. A phase I study of pegylated recombinant arginase (PEG-BCT-100) in combination with systemic chemotherapy (capecitabine and oxaliplatin)[PACOX] in advanced hepatocellular carcinoma patients. *Invest New Drugs* **40**, 314–321. <https://doi.org/10.1007/s10637-021-01178-3> (2022).
15. Abou-Alfa, G. K. et al. Phase III randomized study of second line ADI-PEG 20 plus best supportive care versus placebo plus best supportive care in patients with advanced hepatocellular carcinoma. *Ann Oncol* **29**, 1402–1408. <https://doi.org/10.1093/annonc/mdy101> (2018).
16. Chan, S. L. et al. A phase II clinical study on the efficacy and predictive biomarker of pegylated recombinant arginase on hepatocellular carcinoma. *Invest New Drugs* **39**, 1375–1382. <https://doi.org/10.1007/s10637-021-01111-8> (2021).
17. Feng, T. et al. The arginine metabolism and its deprivation in cancer therapy. *Cancer Lett* **620**, 217680. <https://doi.org/10.1016/j.canlet.2025.217680> (2025).
18. Zou, S., Wang, X., Liu, P., Ke, C. & Xu, S. Arginine metabolism and deprivation in cancer therapy. *Biomed Pharmacother* **118**, 109210. <https://doi.org/10.1016/j.biopha.2019.109210> (2019).
19. Fiedler, T. et al. Arginine deprivation by arginine deiminase of *Streptococcus pyogenes* controls primary glioblastoma growth in vitro and in vivo. *Cancer Biol Ther* **16**, 1047–1055. <https://doi.org/10.1080/15384047.2015.1026478> (2015).
20. Hajji, N. et al. Arginine deprivation alters microglial polarity and synergizes with radiation to eradicate non-arginine-auxotrophic glioblastoma tumors. *J. Clin. Invest.* <https://doi.org/10.1172/JCI142137> (2022).
21. Przystal, J. M. et al. Efficacy of arginine depletion by ADI-PEG20 in an intracranial model of GBM. *Cell Death Dis.* **9**, 1192. <https://doi.org/10.1038/s41419-018-1195-4> (2018).
22. Khoury, O. et al. Human recombinant arginase I (Co)-PEG5000 [HuArgI (Co)-PEG5000]-induced arginine depletion is selectively cytotoxic to human glioblastoma cells. *J. Neurooncol.* **122**, 75–85. <https://doi.org/10.1007/s11060-014-1698-5> (2015).
23. Sun, S. et al. Endoplasmic reticulum chaperone prolyl 4-hydroxylase, beta polypeptide (P4HB) promotes malignant phenotypes in glioma via MAPK signaling. *Oncotarget* **8**, 1911–19123. <https://doi.org/10.18632/oncotarget.18026> (2017).
24. Kwong-Lam, F. & Chi-Fung, C. G. Vincristine could partly suppress stromal support to T-ALL blasts during pegylated arginase I treatment. *Exp. Hematol. Oncol.* **2**, 11. <https://doi.org/10.1186/2162-3619-2-11> (2013).
25. Kanehisa, M. Toward understanding the origin and evolution of cellular organisms. *Protein Sci.* **28**, 1947–1951. <https://doi.org/10.1002/pro.3715> (2019).
26. Kanehisa, M., Furumichi, M., Sato, Y., Kawashima, M. & Ishiguro-Watanabe, M. KEGG for taxonomy-based analysis of pathways and genomes. *Nucleic Acids Res* **51**, D587–D592. <https://doi.org/10.1093/nar/gkac963> (2023).
27. Anakha, J. et al. Human arginase 1, a Jack of all trades?. *3 Biotech* **12**, 264. <https://doi.org/10.1007/s13205-022-03326-9> (2022).
28. de Sena, L. W. P. et al. Doses of chloroquine in the treatment of malaria by *Plasmodium vivax* in patients between 2 and 14 years of age from the Brazilian Amazon basin. *Malar J* **18**, 439. <https://doi.org/10.1186/s12936-019-3072-8> (2019).
29. Chen, C. L., Hsu, S. C., Ann, D. K., Yen, Y. & Kung, H. J. Arginine signaling and cancer metabolism. *Cancers (Basel)* <https://doi.org/10.3390/cancers13143541> (2021).
30. Scalise, M. et al. Membrane transporters for amino acids as players of cancer metabolic rewiring. *Cells* <https://doi.org/10.3390/cel1s9092028> (2020).
31. Chu, Y. D., Lai, M. W. & Yeh, C. T. Unlocking the potential of arginine deprivation therapy: Recent breakthroughs and promising future for cancer treatment. *Int. J. Mol. Sci.* <https://doi.org/10.3390/ijms241310668> (2023).
32. Olafson, L. R., Gunawardena, M., Nixdorf, S., McDonald, K. L. & Rapkins, R. W. The role of TP53 gain-of-function mutation in multifocal glioblastoma. *J. Neurooncol.* **147**, 37–47. <https://doi.org/10.1007/s11060-019-03318-5> (2020).
33. De Souza, C. et al. Effect of the p53 P72R polymorphism on mutant TP53 allele selection in human cancer. *J. Natl. Cancer Inst.* **113**, 1246–1257. <https://doi.org/10.1093/jnci/djab019> (2021).
34. Cheng, C. T. et al. Arginine starvation kills tumor cells through aspartate exhaustion and mitochondrial dysfunction. *Commun. Biol.* **1**, 178. <https://doi.org/10.1038/s42003-018-0178-4> (2018).
35. Artykov, A. A. et al. Death receptors DR4 and DR5 undergo spontaneous and ligand-mediated endocytosis and recycling regardless of the sensitivity of cancer cells to TRAIL. *Front Cell Dev. Biol.* **9**, 733688. <https://doi.org/10.3389/fcell.2021.733688> (2021).
36. Snajdauf, M. et al. The TRAIL in the treatment of human cancer: An update on clinical trials. *Front Mol. Biosci.* **8**, 628332. <https://doi.org/10.3389/fmolb.2021.628332> (2021).
37. Wang, Z. et al. Amino acid degrading enzymes and autophagy in cancer therapy. *Front Pharmacol.* **11**, 582587. <https://doi.org/10.3389/fphar.2020.582587> (2020).
38. Lam, S. K. et al. Inhibition of ornithine decarboxylase 1 facilitates pegylated arginase treatment in lung adenocarcinoma xenograft models. *Oncol. Rep.* **40**, 1994–2004. <https://doi.org/10.3892/or.2018.6598> (2018).
39. Kelly, M. P. et al. Arginine deiminase PEG20 inhibits growth of small cell lung cancers lacking expression of argininosuccinate synthetase. *Br. J. Canc.* **106**, 324–332. <https://doi.org/10.1038/bjc.2011.524> (2012).
40. Leung, S. L. et al. PEGylated recombinant human arginase as a drug for breast cancer. *Hong Kong Med J.* **25**(Suppl 9), 28–31 (2019).
41. Zhao, Z. et al. Pegylated recombinant human arginase 1 induces autophagy and apoptosis via the ROS-activated AKT/mTOR pathway in bladder cancer cells. *Oxid Med. Cell Longev* **2021**, 5510663. <https://doi.org/10.1155/2021/5510663> (2021).
42. Martinet, W., Schrijvers, D. M., Herman, A. G. & De Meyer, G. R. z-VAD-fmk-induced non-apoptotic cell death of macrophages: possibilities and limitations for atherosclerotic plaque stabilization. *Autophagy* **2**, 312–314. <https://doi.org/10.4161/auto.2966> (2006).
43. Wu, Y. T. et al. zVAD-induced necroptosis in L929 cells depends on autocrine production of TNF α mediated by the PKC-MAPKs-AP-1 pathway. *Cell Death Differ* **18**, 26–37. <https://doi.org/10.1038/cdd.2010.72> (2011).
44. Zhang, Y., Chen, X., Gueydan, C. & Han, J. Plasma membrane changes during programmed cell deaths. *Cell Res* **28**, 9–21. <https://doi.org/10.1038/cr.2017.133> (2018).

45. Syed, N. et al. Epigenetic status of argininosuccinate synthetase and argininosuccinate lyase modulates autophagy and cell death in glioblastoma. *Cell Death Dis.* **4**, e458. <https://doi.org/10.1038/cddis.2012.197> (2013).
46. Zhou, W. et al. Chloroquine against malaria, cancers and viral diseases. *Drug Discov Today* **25**, 2012–2022. <https://doi.org/10.1016/j.drudis.2020.09.010> (2020).
47. Jutten, B. et al. EGFRvIII expression triggers a metabolic dependency and therapeutic vulnerability sensitive to autophagy inhibition. *Autophagy* **14**, 283–295. <https://doi.org/10.1080/15548627.2017.1409926> (2018).
48. Verbaanderd, C. et al. Repurposing drugs in oncology (ReDO)-chloroquine and hydroxychloroquine as anti-cancer agents. *Ecancermedicalscience* **11**, 781. <https://doi.org/10.3332/ecancer.2017.781> (2017).
49. Andersen, R. S., Anand, A., Harwood, D. S. L. & Kristensen, B. W. Tumor-Associated microglia and macrophages in the glioblastoma microenvironment and their implications for therapy. *Cancers (Basel)* <https://doi.org/10.3390/cancers13174255> (2021).
50. Khan, F. et al. Macrophages and microglia in glioblastoma: Heterogeneity, plasticity, and therapy. *J Clin Invest* <https://doi.org/10.1172/JCI163446> (2023).
51. Gutmann, D. H. & Kettenmann, H. Microglia/brain macrophages as central drivers of brain tumor pathobiology. *Neuron* **104**, 442–449. <https://doi.org/10.1016/j.neuron.2019.08.028> (2019).
52. Li, J., Law, H. K., Lau, Y. L. & Chan, G. C. Differential damage and recovery of human mesenchymal stem cells after exposure to chemotherapeutic agents. *Br. J. Haematol.* **127**, 326–334. <https://doi.org/10.1111/j.1365-2141.2004.05200.x> (2004).
53. Sultana, S. & Bishayi, B. Etoposide-mediated depletion of peripheral blood monocytes post s.aureus infection attenuates septic arthritis by modulating macrophage-derived factors responsible for inflammatory destruction. *Immunol. Lett.* **220**, 51–62. <https://doi.org/10.1016/j.imlet.2020.02.001> (2020).
54. Menna, G. et al. Glioma-associated microglia characterization in the glioblastoma microenvironment through a “seed-and soil” approach: A systematic review. *Brain Sci.* <https://doi.org/10.3390/brainsci12060718> (2022).

Acknowledgements

Dr. Cheng NM Paul (Bio-Cancer Treatment Ltd., Hong Kong) kindly provided BCT-100. L-luciferin and the AV/PI kit were sponsored by Bio-Cancer Treatment Ltd, Hong Kong. The study was funded by the Hotung Sai Kim Foundation.

Author contributions

Fung MKL designed the research, performed the experiments, analyzed the data, and wrote the manuscript. Chan S assisted in operating the CRI Maestro™ imaging system and orthotopic glioma engraftment. Sun S, Zhang PD, and Leung GKK assisted in the establishment of the orthotopic glioma engraftment platform. Chan GCF designed the research, interpreted the data, and revised and finally approved the manuscript. The author(s) read and approved the final manuscript.

Funding

The study was funded by the Hotung Sai Kim Foundation.

Declarations

Competing interests

The authors declare no competing interests.

Ethics approval

The animal study was approved by the Committee on the Use of Live Animals for Teaching and Research (CULATR) of The University of Hong Kong. All methods were performed in accordance with the relevant guidelines and regulations. All methods are reported in accordance with ARRIVE guidelines.

Additional information

Supplementary Information The online version contains supplementary material available at <https://doi.org/10.1038/s41598-025-13882-8>.

Correspondence and requests for materials should be addressed to G.C.F.C.

Reprints and permissions information is available at www.nature.com/reprints.

Publisher's note Springer Nature remains neutral with regard to jurisdictional claims in published maps and institutional affiliations.

Open Access This article is licensed under a Creative Commons Attribution-NonCommercial-NoDerivatives 4.0 International License, which permits any non-commercial use, sharing, distribution and reproduction in any medium or format, as long as you give appropriate credit to the original author(s) and the source, provide a link to the Creative Commons licence, and indicate if you modified the licensed material. You do not have permission under this licence to share adapted material derived from this article or parts of it. The images or other third party material in this article are included in the article's Creative Commons licence, unless indicated otherwise in a credit line to the material. If material is not included in the article's Creative Commons licence and your intended use is not permitted by statutory regulation or exceeds the permitted use, you will need to obtain permission directly from the copyright holder. To view a copy of this licence, visit <http://creativecommons.org/licenses/by-nc-nd/4.0/>.

© The Author(s) 2025